A Framework for Classification and Segmentation of Branch Retinal Artery Occlusion in SD-OCT

Jingyun Guo, Weifang Zhu, Fei Shi, Dehui Xiang, Haoyu Chen, and Xinjian Chen, *Senior Member, IEEE*

***Abstract*— Branch retinal artery occlusion (BRAO) is an ocular emergency, which could lead to blindness. Quantitative analysis of the BRAO region in the retina is necessary for the assessment of the severity of retinal ischemia. In this paper, a fully automatic framework was proposed to segment BRAO regions based on 3D spectral-domain optical coherence tomography (SD-OCT) images. To the best of our knowledge, this is the first automatic 3D BRAO segmentation framework. First, the input 3D image is automatically classified into BRAO of acute phase and BRAO of chronic phase or normal retina using an AdaBoost classifier based on combining local structural, intensity, textural features with our new feature distribution analyzing strategy. Then, BRAO regions of acute phase and chronic phase are segmented separately. A thickness model is built to segment BRAO in the chronic phase. While for segmenting BRAO in the acute phase, a two-step segmentation strategy is performed: rough initialization and refine segmentation. The proposed method was tested on SD-OCT images of 35 patients (12 BRAO acute phase, 11 BRAO chronic phase, and 12 normal eyes) using the leave-one-out strategy. The classification accuracy for BRAO acute phase, BRAO chronic phase, and normal retina were 100%, 90.9%, and 91.7%, respectively. The overall true positive volume fraction (TPVF) and false positive volume fraction (FPVF) for the acute phase were 91.1% and 5.5% and for the chronic phase were 92.7% and 8.4%, respectively.**

***Index Terms*— Branch retinal artery occlusion, AdaBoost classifier, graph search-graph cut, segmentation, Bayesian posterior probability.**

I. Introduction

BRANCH retinal artery occlusion (BRAO) is a potentially devastating visual disorder usually caused by closure of the vessel [1], [2]. It disrupts nutrition supply of the corresponding retinal area, resulting in edemain affected retinal sectors because of ischemia and anoxia [2]–[4]. Patients with BRAO usually suffer from sudden segmental visual loss. It may lead to completely blindness if the patient can't get timely treatment. Commonly, BRAO occurs secondary to an embolus in a branch vessel which is visible only in 20% of the patients with BRAO [5]. Therefore, research of the edema tissue of BRAO has a great value for the diagnosis and treatment of BRAO patients.

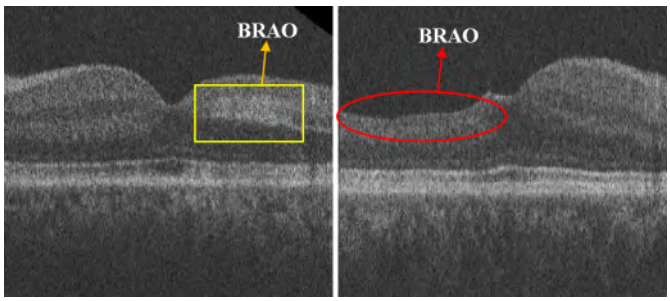

(a) (b)

Fig. 1. Illustrations for BRAO in SD-OCT images. (a) A slice of the original image in acute phase. BRAO results in local edema and has a high intensity as marked in yellow rectangle; (b) A slice of the original image in chronic phase. BRAO results thickness decrease and texture fuzzy in inner retina as marked in red ellipse.

Optical coherence tomography (OCT) was recently widely used in ophthalmology, which could provide in vivo, non-invasive, cross-sectional images of the retina. It has been described to show the high reflectivity corresponding to the edematous inner retina layers and hyporeflective signal from the photoreceptor layer. However, the resolution of the images on conventional time-domain OCT is not adequate to resolve the changes in individual layers of the retina [6]. Spectral-domain OCT (SD-OCT) by its ability to acquire a large number of images in a short period of time provides high resolution images [7], [8].

It was reported that BRAO is characterized histopathologically by inner retinal edema initially, called acute phase and atrophy in the presence of persistent ischemia, called chronic phase [9]. In the acute phase, optical reflectivity in OCT image increases in inner retina and correspondingly decreases in outer retina; while in the chronic phase, the inner retina atrophy and its thickness reduces [6], [10], as shown in Fig. 1. Studies have shown that the volume of the blocked spaces in retina can be an accurate predictor of visual acuity (VA). Further, clinical studies based on the volume of BRAO region may be used as a metric for visual prognosis and is important

Manuscript received June 25, 2016; revised December 5, 2016 and January 19, 2017; accepted April 16, 2017. Date of publication April 25, 2017; date of current version May 26, 2017. This work was supported in part by the National Basic Research Program (973), the Young Scientist Program Foundation of China, under Grant 2014CB748600, in part by the National Nature Science Foundation of China for Excellent Young Scholars under Grant 61622114, in part by the National Natural Science Foundation of China under Grant 81401472, Grant 61401293, Grant 61401294, and Grant 81371629, and in part by the Natural Science Foundation of the Jiangsu Province under Grant BK20140052. The associate editor coordinating the review of this manuscript and approving it for publication was Prof. Chunming Li. *(Corresponding author: Xinjian Chen.) (Jingyun Guo and Weifang Zhu contributed equally to this work.)*

J. Guo, W. Zhu, F. Shi, D. Xiang, and X. Chen are with the School of Electronics and Information Engineering, Soochow University Suzhou 215000, China (e-mail: jingyunguo1992@foxmail.com; wfzhu@suda.edu.cn; shifei@suda.edu.cn; xiangdehui@suda.edu.cn; xjchen@suda.edu.cn).

H. Chen is with the Joint Shantou International Eye Center, Shantou University, Shantou 515063, China, and also with the Chinese University of Hong Kong, Shantou 515063, China (e-mail: drchenhaoyu@gmail.com).

Color versions of one or more of the figures in this paper are available online at http://ieeexplore.ieee.org.

Digital Object Identifier 10.1109/TIP.2017.2697762

for clinicians to make a plan for conservative treatment. However, in clinical practice, the diagnosis of BRAO is quite qualitative and subjective.

Several approaches have been introduced to diagnosis BRAO quantitatively, but none of them could evaluate occlusion volume and size. For instance, Chen *et al.* [11] proposed a framework to analyze the retinal layer intensity of BRAO based on 3D OCT image. Leung *et al.* [12] measured the macular and peripapillary retinal nerve fiber layer (RNFL) thickness and visual sensitivity to investigate the structure–function relationship in patients with BRAO, which was done manually and roughly. Asefzadeh and Ninyo [13] analyzed the longitudinal retinal changes of the peripapillary RNFL thickness of BRAO.

In this paper, we propose a fully automated and efficient method to detect and segment BRAO region. To the best of our knowledge, this is the first automatic 3D BRAO segmentation framework. In this work, BRAO of acute phase and chronic phase are differentiated from normal eyes based on a nice designed AdaBoost classifier, and then the BRAO regions are segmented respectively. Furthermore, this method generates the 2D projections of BRAO regions, which could provide shape, size and position information to aid the ophthalmologist's diagnosis.

Our contributions are summarized as follows:

- An effective 3D automatic framework is proposed to detect and segment BRAO in retinal SD-OCT images.
- An AdaBoost classifier is designed to differentiate BRAO of acute phase, BRAO of chronic phase and normal retina combining local features with our new feature distribution analyzing strategy.
- For segmenting BRAO in acute phase, a two-step graph based segmentation is proposed, which contains the Bayesian posterior probability based initialization, and an advanced graph search-graph cut (GSGC) method based segmentation method.
- For the chronic phase, an efficient thickness model is built to segment lesion areas.

II. Related Work

A. Retinal Tissue or Disease Segmentation in OCT

Retinal tissue or disease segmentation in OCT has been very popular in ophthalmology research, such as retinal vessel segmentation [14]–[16], pigment epithelial detachment (PED) segmentation [17], [18], IS/OS (inner segment/outer segment) disruption detection and macular hole segmentation [19], or other diseases or tissues. The most commonly used methods are graph cut, graph search, random walk, AdaBoost classifier and random forest.

Segmentation of tissue or disease in SD-OCT is a challenging task because of complexity and diversity: (1) shape and size of the interest regions are various; (2) there are no clear boundaries between the interest regions and the surrounding tissues; (3) OCT image quality is also easily influenced by noise or other factors. Therefore, traditional graph cut and graph search method may not be competent for segmentation in OCT images.

B. Graph Cut and Graph Search Method

Graph cut method has been widely used in various segmentation problems in recent years. The main idea of GC is computing a minimum cost s/t cut on a directed constructed graph based on an energy function, which includes regional term and boundary term [20]–[28].

Graph search methods [17], [29]–[33] work very well for the segmentation of terrain-like surfaces and suggest representing the terrain-like surface as a related closed set. The approach is able to segment the terrain-like surface through constructing an optimal closed set. A corresponding sub-graph for each surface is constructed for multiple-surface segmentation, which can be solved simultaneously as a single s/t cut problem by using a maximum-flow/minimum-cut algorithm [25].

Our work is motivated by Chen's method [34]. In Chen's method, the aim is to segment symptomatic exudate-associated derangements (SEAD). In this paper, our aim is to segment BRAO. BRAO has two types, which have completely different texture and shape. So we propose a new framework to differentiate BRAO of acute and chronic phase based on an AdaBoost classifier. For BRAO in chronic phase, a thickness model is built to segment BRAO region. For BRAO in acute phase, the segmentation is based on the GSGC method. A preliminary version of this work has been published in [35]. We extend this previous work by incorporating local structural, intensity and textural features in the classification step. In addition, we improve segmentation for BRAO chronic phase by using a thickness model.

III. Methods

A. Method Overview

The proposed method comprises four parts (Fig. 2). First, pre-processing steps are applied which contains layer segmentation, flatten and de-noising. Then, an AdaBoost classifier is designed to differentiate three types of images (normal, BRAO of acute phase, BRAO of chronic phase). Then, BRAO regions of acute phase and chronic phase are segmented separately. To segment BRAO in chronic phase, a thickness model is built. While for segmenting BRAO in acute phase, a two-step segmentation strategy is applied: rough initialization and refine segmentation. During the initialization phase, the Bayesian posterior probability is utilized to compute the probability map. In the segmentation phase, an advanced graph-search-graph-cut method is applied to segment the BRAO regions, in which the initialization results are fully utilized as the constraints when constructing the energy function.

B. Pre-Processing

1) Layer Segmentation and Flatten: Intra-retinal layer segmentation is essential for accurately lesion location and segmentation. In this paper, the OCT image is segmented automatically using the multi-layer graph search based method [29], yielding 11 surfaces (10 layers): retinal nerve fiber layer (RNFL), ganglion cell layer (GCL), inner plexiform layer (IPL), inner nuclear layer (INL), outer plexiform layer (OPL), outer nuclear layer (ONL), inner segment layer (ISL),

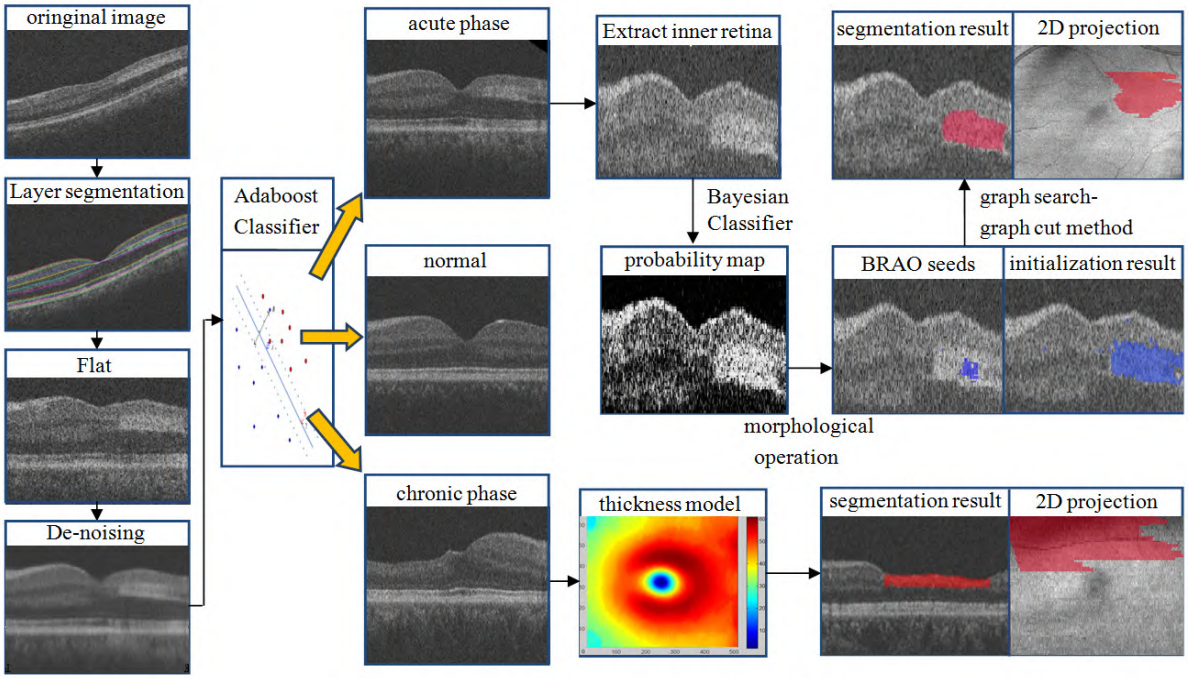

Fig. 2. Flowchart of BRAO classification and segmentation in SD-OCT.

connecting cilia (CL), outer segment layer (OSL), Verhoeff's membrane (VM), and retinal pigment epithelium (RPE) [17]. The cost function is described as:

$$E = \sum_{v \in S} C_v + \sum_{(p,q) \in N} w_{p,q}(S(p) - S(q)), \qquad (1)$$

where S is the desired surface, C_v is an edge-based cost, which is inversely related to the likelihood that S contains the voxel v,(p, q) is a pair of neighboring columns N, $w_{p,q}$ is a convex function penalizing the surface S shape change on p and q.

It is reported that layer segmentation methods work well in normal retina OCT images, but in some cases when there are dramatic changes in the layer structure, the layer segmentation results are not satisfactory [17], [36]. In this paper, even though the thickness or intensity has changed in BRAO images, surface 1, 6, 7, and 11 are still clear, and the segmentation performance is not affected, as shown in Fig. 3 (a) (b).

Then, the OCT image is flattened based on the bottom layer of RPE. Fig. 3 (c) shows a flattened macular centered OCT B-scan with the layer segmenting result overlaid on it, 11 surfaces defining 10 retinal layers. In this paper, inner retina refers to the layers between surface 1 and surface 6, and outer retina refers to the layers between surface 7 and surface 11.

2) De-Noising by an Anisotropic Diffusion Filter: The speckle noise is usually existed in SD-OCT images, which affects the effectiveness of segmentation and feature extraction due to the intensity discontinuity. However, edge and noise are both high-frequency signals, it is difficult to make a decision in the noise and edges. So, most de-noising methods are often unsatisfactory in terms of anti-noise performance and edge preserving. In this paper, the anisotropic diffusion method is applied and which can accomplish both edges-preserving and noise-removing. It has been widely used in speckle reduction [37]–[41]. The diffusion equation for the anisotropic diffusion

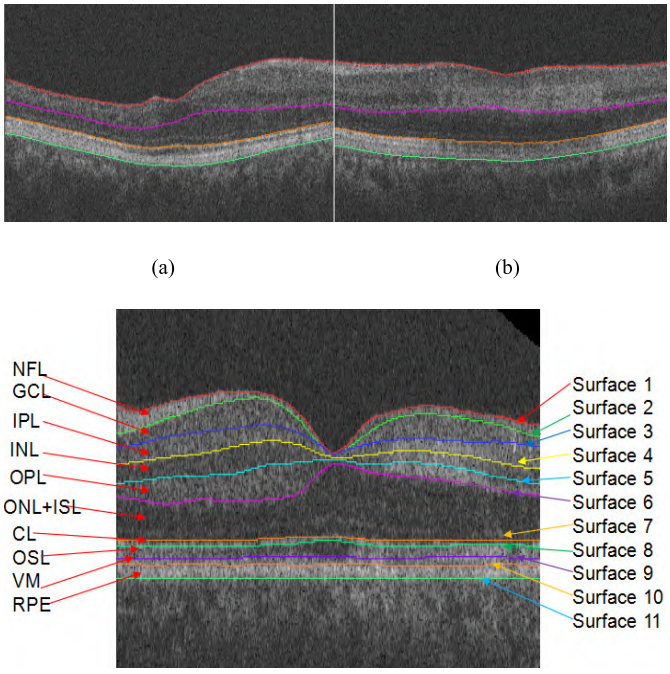

Fig. 3. Illustrations for layer segmentation results for BRAO. (a) B-scan image of BRAO acute phase with surface 1, 6, 7, and 11 on it. (b) B-scan image of BRAO chronic phase with surface 1, 2, 6, 7, and 11 on it. (c) The segmented 11 surfaces overlaid on the OCT image.

filter can be written as [42]:

$$\frac{\partial I}{\partial t} = div[c(|\nabla I|) \cdot \nabla I], \qquad (2)$$

where I is the input image, div is the divergence operator, $|\nabla I|$ is the diffusion coefficient, ∇ is the gradient operator.

TABLE I
USED CLASSIFICATION FEATURES

Features No	Feature Description
1	The thickness of inner retina
2	Voxel intensity
3-34	Co-occurrence matrix energy, entropy, inertia and correlation of 8 directions
35-50	Output of a Gabor filter including two center frequency and eight directions

C. AdaBoost Based BRAO Classification

Since BRAO has acute phase and chronic phase, it is necessary to differentiate the two types. In this paper, the AdaBoost classifier is applied based on texture and shape features. And these local voxel features are combined with our new feature distribution analyzing strategy to construct the global image feature set.

1) Local Features: In this paper, for each voxel, 50 features are calculated describing the structural, intensity, and textural characteristics (Table I), which correspond to 50 3D feature images. Structural feature (1) describes the local inner retina thickness while intensity feature (2) describes local intensity. Co-occurrence matrix (3-34) and Gabor filter (35-50) are used to describe voxel texture, where the co-occurrence matrix energy, entropy, inertia, correlation are calculated in 8 directions, and Gabor filter is performed with two center frequencies and eight directions. For each feature image (except feature 1), inner retina volume and outer retina volume are extracted and then analyzed respectively, yielding 99 3D feature images.

The inner retina thickness is a very important feature because that inner retina thickness decrease is the only judgment criteria for BRAO chronic phase. While inner retina and outer retina intensity change is the most obvious characteristic of BRAO acute phase. Both BRAO acute phase and chronic phase show texture changes in BRAO regions. In this paper, we apply two popular voxel texture description methods: co-occurrence matrix and Gaber filter. Where, Co-occurrence matrix has been demonstrated to be effective to describe local texture in SD-OCT images [34], [43].

2) Feature Distribution Analysis: As BRAO occurs in the branch retinal artery, resulting structural or textural changes only in the corresponding regions, which reflects in irregular parts in feature distribution maps. Intra B-scans variations are obvious, as shown in Fig. 1. Inter B-scans variations are described in Fig. 4 by calculating the mean of feature in each B-scan, which can intuitively reflect the lesion area. As shown in the first column of Fig. 4, the changing curve of inner retina intensity for normal retina and retina with BRAO in chronic phase are similar, both show a Gaussian-like distribution, as described in the black curves. The inner retina intensity increasing in BRAO acute phase happens in different parts of the 64 B-scans, as described in the red curves. Irregular variation for images with BRAO is also obvious for thickness (second column of Fig. 4) and other features. So, a feature distribution analyzing strategy is proposed to capture these feature variations. First, the whole volume is divided into 12

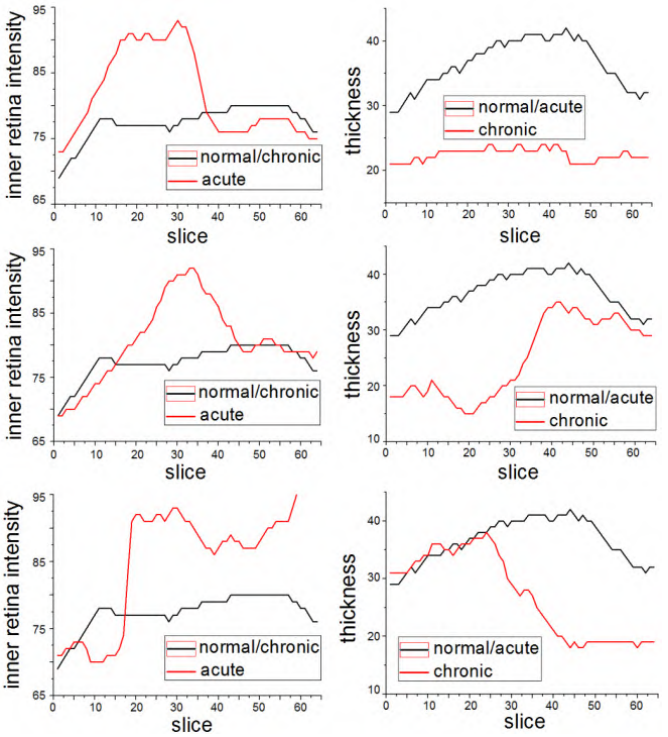

Fig. 4. Illustration of examples of feature changing curve during the 64 continuous B-scans. The first column shows three examples of inner retina intensity; the second column shows three examples of thickness.

consecutive sub-volumes to describe small variations (Fig. 5), and the mean and standard deviation of each sub-volume are calculated. We choose this scale in consideration of the size of BRAO region. Second, 6 properties are designed by analyzing the 12 sub-volumes, which can capture both large and small variations of features. The six properties are designed as follows:

a) The maximum of the 12 sub-volumes: $F_1 = \max_{i,j}(V_{ij})$;
b) The minimum of the 12 sub-volumes: $F_2 = \min_{i,j}(V_{ij})$;
c) The maximum difference between the 12 sub-volumes: $F_3 = \max_{i,j}(V_{ij}) - \min_{i,j}(V_{ij})$;
d) The mean of the whole 12 sub-volumes: $F_4 = \sum_{i=1}^{4}\sum_{j=1}^{3} V_{ij}$;
e) The maximum difference in the X direction: $F_5 = \max_{i}\left\{\max_{j}(V_{ij}) - \min_{j}(V_{ij})\right\}$;
f) The maximum difference in the Y direction: $F_6 = \max_{j}\left\{\max_{i}(V_{ij}) - \min_{i}(V_{ij})\right\}$.

Where, V_{ij} represents the mean or standard deviation of the sub-volume; i is the index number in the X direction and j is the index number in the Y direction.

Third, the six properties are calculated for both mean and standard deviation respectively, yielding 12 descriptors for each of the 99 feature images, constituting the global feature set which are used to differentiate three types of images (normal, BRAO of acute phase, BRAO of chronic phase). So, a total of 1188 (99 multiplies 12) features are used to characterize each retina.

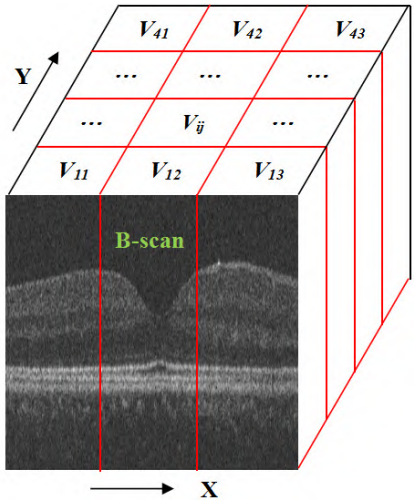

Fig. 5. Illustration of the 12 consecutive sub-volumes.

3) Classification Using AdaBoost Classifier: After computing the global feature set, the AdaBoost classifier [44] is applied to identify BRAO acute phase, BRAO chronic phase and normal retina. AdaBoost combines a set of weak classifiers in order to form an ensemble classifier. In this paper, we use threshold classifier as weak classifier, and one 2-class weak classifier for one feature. At last, we train three ensemble classifiers for normal retina, BRAO acute phase and BRAO chronic phase, respectively. And each of them is used independently.

D. Segmentation of BRAO in Acute Phase

Segmentation of BRAO in acute phase is a challenging task because of its complexity and diversity. Therefore, an accurate region segmentation method is needed. Our proposed segmentation of BRAO in acute phase method includes two main parts: initialization and segmentation. In the initialization step, the Bayesian posterior probability is used to initialize segmentation. In the segmentation step, an advanced graph based GSGC method is applied in which graph cut and graph search methods are fully integrated.

1) Bayesian Based Probability Initialization: Due to the intensity increasing only occurs between surface 1 and surface 6 (inner retina) in acute phase, the inner retina from the original image is extracted based on the segmented layers. This can avoid the interference of high intensity voxels between surface 7 and surface 11 (outer retina) and reduce the running time in the segmentation step. To initialize the BRAO segmentation algorithm, the Bayesian posterior probability is calculated to assign a likelihood to each voxel that it belongs to BRAO region.

During the training step, voxels between surface 1 and surface 6 are used as set S. Each voxel in S is labeled as occlusion l_o or normal l_n according to the reference standard. The probability for a voxel v_i belonging to the BRAO region is calculated using Equation (3).

$$P(v_i \in R_o|I_{\mathrm{p}}) = \frac{P(I_P|R_o)\cdot P(R_o)}{P(I_P|R_o)\cdot P(R_o) + P(I_P|R_n)\cdot P(R_n)}, \tag{3}$$

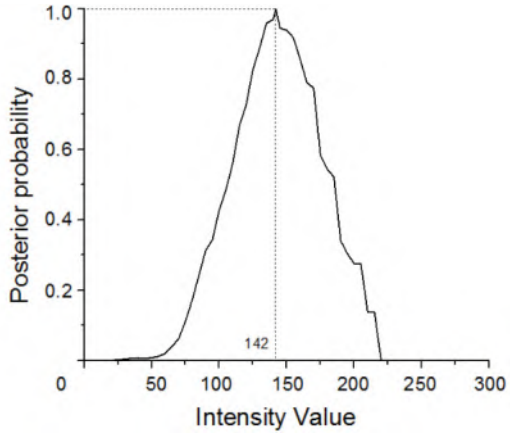

Fig. 6. Probability that a voxel belongs to BRAO region.

with

$$p(R_o) = \frac{hist(l_i \in l_o, v_i \in S)}{hist(v_i \in S)}, \tag{4}$$

$$p(R_n) = \frac{hist(l_i \in l_n, v_i \in S)}{hist(v_i \in S)}, \tag{5}$$

$$p(I_P|R_o) = \frac{hist(l_i \in l_o, v_i \in R_{\mathrm{o}})}{hist(v_i \in R_o)}, \tag{6}$$

$$p(I_P|R_{\mathrm{n}}) = \frac{hist(l_i \in l_o, v_i \in R_{\mathrm{n}})}{hist(v_i \in R_{\mathrm{n}})}, \tag{7}$$

where, I_p represents the voxel intensity, which varies from 0 to 255, R_o represents occlusion region and R_n represents non-occlusion region. The probability of R_o is the percentage of voxels in S labeled with l_o in all voxels and the probability of R_n is the percentage of voxels in S labeled with l_n. $P(I_p|R_o)$ and $P(I_p|R_n)$ represent the probability that the intensity of a voxel equals to I_p in the occlusion and non-occlusion region, respectively. These probability are calculated by analyzing the voxel intensity distribution of occlusion regions and non-occlusion regions in the reference standard. Fig. 6 shows the calculated Bayesian posterior probability.

For the input testing image, the posterior probability is calculated and each voxel between surface 1 and 6 is assigned a likelihood between 0 and 1. The probability map will serve as a constraint in the latter segmentation step.

After obtaining the probability map, several post-processing steps are applied to get the final initialization result. First, the mean filter is used to smooth the image. Second, the high likelihood voxels (over 0.5, the median value) are set as BRAO region. Third, RNFL is removed because of its high intensity according to the segmented layers. Finally, initialization results are obtained by morphological closing and opening operations, in which closing fills up black blobs inside BRAO regions, and opening removes the small and isolated points outside BRAO regions.

2) Graph-Search-Graph-Cut Based BRAO Segmentation: The GSGC method had been proposed for retinal fluid segmentation and achieved good results [34]. The method effectively combines the graph search and graph cut methods for segmenting the layers and regions simultaneously. The whole

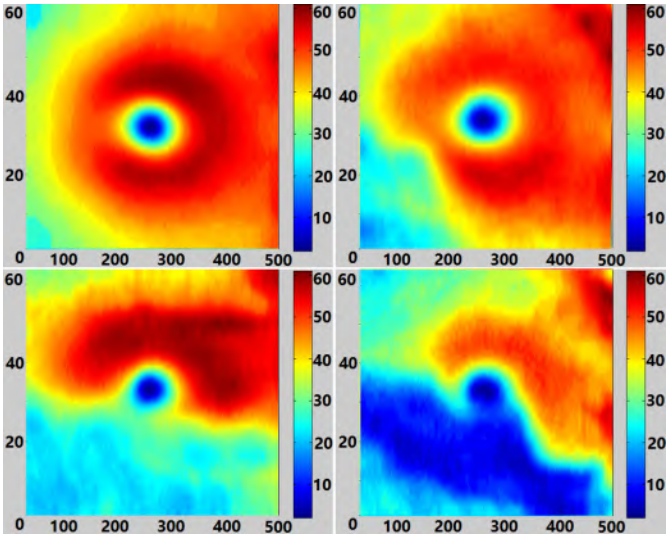

Fig. 7. Illustration of the thickness model. The first picture shows the mean of the normal retina thickness model. The other three pictures shows three different examples of thickness model of BRAO in chronic phase.

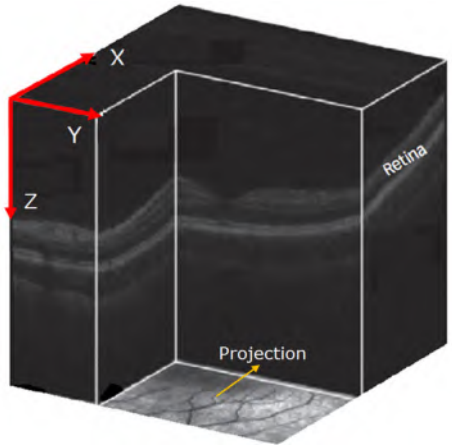

Fig. 8. Illustration of a 3D OCT image with its projection.

energy cost function is designed as:

$$En(f) = E(Surfaces) + E(Regions) + E(Interactions), \tag{8}$$

where *E(Surfaces)* represents the cost associated with the segmentation of the surfaces, *E(Regions)* represents the cost associated with the segmented regions, and *E(Interactions)* represents the cost of constraints between the surfaces and regions. The initialization results are used as the constraints in *E (Regions)*, defined as follows,

$$E = \sum_{p \in P} (\alpha \cdot D_p(f_p) + \beta \cdot C_p(f_p)) + \sum_{p \in P, q \in N_p} \gamma \cdot B_{p,q}(f_p, f_q), \tag{9}$$

where α, β, γ are the weights for the data term, probability constrained term, and boundary term, respectively.

$$C_p(f_p) = 1 - \exp(-\lambda \cdot InitP(p)), \tag{10}$$

TABLE II

CLASSIFICATION PERFORMANCE OF ADABOOST CLASSIFIER DIFFERENTIATING BRAO OF ACUTE PHASE AND CHRONIC PHASE. THE FIRST ROW REPRESENTS THE TRUE CLASS AND THE FIRST COLUMN REPRESENTS CLASSIFICATION RESULT

True Class / Classification Results	Acute phase	Chronic phase	Normal
Acute phase	12	0	1
Chronic phase	0	10	0
Normal	0	1	11
Accuracy	100%	90.9%	91.7%

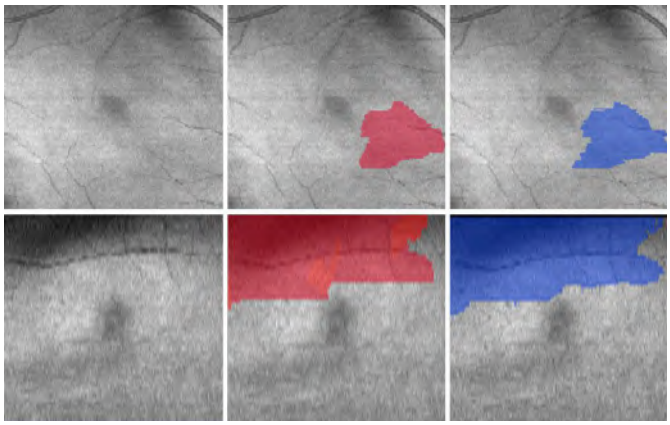

Fig. 9. Two examples of 2D projection of BRAO regions. The first row shows an example of BRAO in acute phase, the 2nd row shows an example of BRAO in chronic phase. The 1st, 2nd, 3rd columns correspond to 2D projections of the original image, segmentation results and ground truth, respectively.

where *InitP(p)* is the probability of voxel p which is from the probability map in the initialization step.

The initialization results are also used to generate BRAO object and background seeds. The BRAO object seeds are generated using morphologic operation of erosions, and the background seeds are generated using morphologic operation of dilations.

E. Segmentation of BRAO in Chronic Phase

In chronic phase, optical intensity is normal in both inner and outer retina, but retinal thickness decreases in inner retina. However, the inner retina thickness varies in different place related to the position to the macula. Hence, the GSGC based segmentation method is not appropriate here and a model-based method is proposed to segment BRAO in chronic phase. The thickness model is built based on a set of macula-centered 3D-OCT images based on the inner retina thickness. First, we adjust the retina position by shifting the fovea to the center of the 3D SD-OCT image. The fovea is located automatically by applying a small threshold to inner retina thickness. The thickness smaller than the threshold correspond to the fovea. Because there are differences between left and right eyes, we apply symmetry operation to remove the differences. Second, for each column in the Z direction, the distance between surface 1 and surface 6 is recorded in its macula-centered

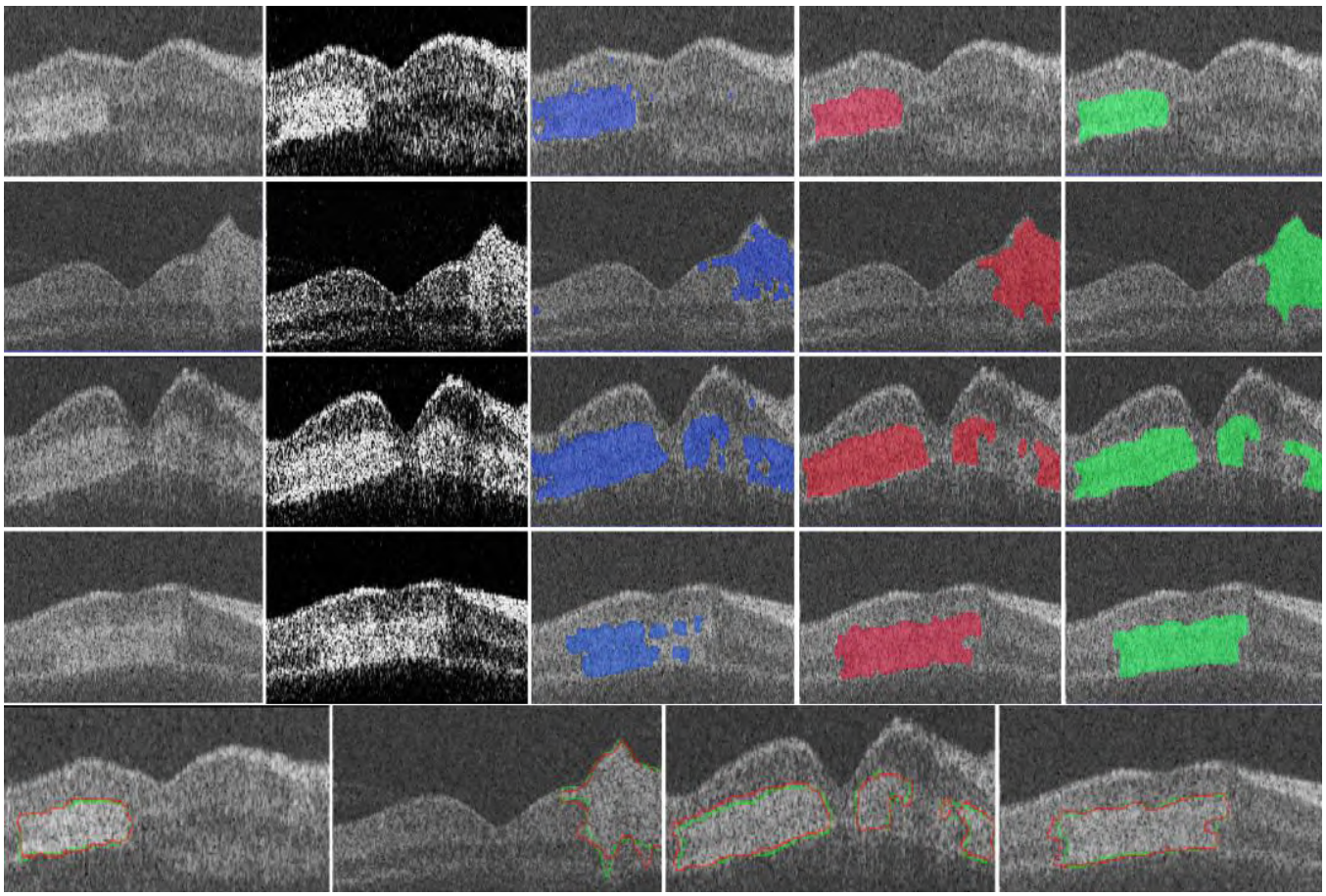

Fig. 10. Segmentation results for f BRAO examples in acute phase. The first column shows the original images, the 2nd column shows the probability maps, the 3rd column shows the initialization results, the 4th column shows the final segmentation results, and the last column shows the ground truth. The last row shows edge of the segmentation results (red curve) and ground truth (green curve).

position *(x, y) (x = 1, 2,.., X; y = 1, 2,.., Y)* in the thickness model, as shown in Fig. 7. In this paper, twenty normal retina images are used to calculate the average normal retina model, generating the mean $e_{x,y}$ and standard deviation $\mu_{x,y}$ of the thickness. Third, the thickness model is fitted to each retina with BRAO in chronic phase to get the BRAO regions. If the thickness $T_{x,y}$ in position *(x, y)* satisfies equation (11), the corresponding tissue is considered as BRAO region, otherwise, it is normal.

$$T_{x,y} < e_{x,y} - \mu_{x,y} \tag{11}$$

In clinics, the ophthalmologist usually diagnoses the BRAO in chronic phase by viewing the 2D projection image. Therefore, we project the 3D OCT volumes into 2D images. Voxels in each Z direction in the whole retina (from surface 1 to surface 11) are averaged, displaying in corresponding position in the 2D projection images, as shown in Fig. 8. Simultaneously, the segmented BRAO volumes are also projected and overlaid on the 2D projection of original images.

IV. Experimental Results

A. Subject Data and Reference Standard

Macula-centered SD-OCT scans of 23 eyes from 23 subjects diagnosed with BRAO (12 of acute phase and 11 of chronic phase) were acquired using Topcon 3D-OCT comprised of

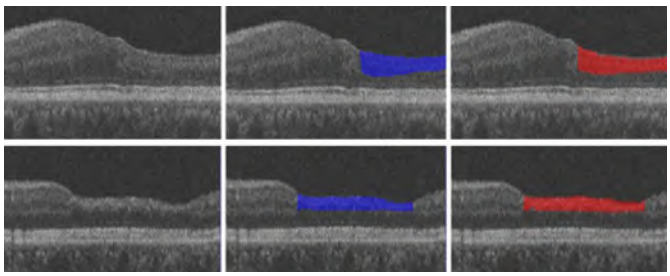

Fig. 11. Segmentation results for two BRAO examples in chronic phase. The 1^{st},2^{nd},3^{rd} columns correspond to original images, segmentation results and ground truth, respectively.

512 × 64 × 480 voxels with voxel size of 11.72 × 93.75 × 3.50 μm^3 or 512 × 128 × 480 voxels with voxel size of 11.72 × 46.88 × 3.50 μm^3 and volume of OCT scan is 6 × 6 × 1.68 mm^3. The latter is first down sampled by a factor of 2 in the Y directions, yielding overall images sized 512 × 64 × 480 voxels. This study is approved by the Intuitional review board of Joint Shantou International Eye Center and adhered to the tenets of the Declaration of Helsinki.

To evaluate the performance of the proposed algorithm, BRAO regions are labeled in each slice of all subjects (supervised by an experienced ophthalmologist), and the results are used as ground truth. The leave-one-out strategy is applied for AdaBoost classifier and Bayesian probability initialization.

TABLE III

MEAN ± STANDARD DEVIATION OF TPVF, FPVF AND ACC OF INITIALIZATION RESULT, TRADITIONAL GC (WITH SAME INITIALIZATION COMPARED TO THE PROPOSED METHOD), GSGC (WITHOUT INITIALIZATION) AND THE PROPOSED METHOD FOR SEGMENTATION OF ACUTE PHASE

	TPVF(%)	FPVF(%)	ACC(%)
Initialization	73.4±14.6	24.0±9.3	88.3±2.8
Traditional GC[46]	79.4±7.6	20.2±4.9	95.0±1.5
GSGC	89.1±3.6	7.9±3.9	95.3±1.1
Proposed method	91.1±2.4	5.5±3.6	97.5±1.2

B. Assessment of the Classification Performance

For classification, 12 normal eyes are included into the dataset, and the leave-one-out strategy is used for evaluation. As shown in Table II, the classification accuracy of AdaBoost classifier is 94.3%, in which 33 out of 35 eyes are correctly classified.

C. Assessment of the Segmentation Performance

Fig. 9 shows 2D projection of BRAO regions in acute phase and chronic phase. Compared with ground truth, we can see that segmentation of BRAO regions is good.

The true positive volume fraction (TPVF), false positive volume fraction (FPVF) and accuracy (ACC) are used to evaluate the segmentation performance, which are calculated as follows,

$$\text{TPVF} = \frac{V_{TP}}{V_{TP} + V_{FN}}, \tag{12}$$

$$\text{FPVF} = \frac{V_{FP}}{V_{FP} + V_{TN}}, \tag{13}$$

$$\text{ACC} = \frac{V_{TP} + V_{TN}}{V_{TP} + V_{FP} + V_{TN} + V_{FN}}, \tag{14}$$

where, V_{TP}, V_{FP}, V_{TN} and V_{FN} represents true positive, false positive, true negative and false negative, respectively. More details can be seen in [45].

Fig. 10 and Fig. 11 show 6 segmentation results of BRAO (4 of acute phase and 2 of chronic phase). TPVF and FPVF for chronic phase are 92.7% and 8.4%; and for acute phase are 91.1%, 5.5%, respectively.

To show the significance of the Bayesian posterior probability constrained GSGC method for segmentation in BRAO acute phase, we compare the proposed graph based method with the initialization result, traditional GC method [46] and Graph-Search-Graph-Cut method (without initialization), where the initialization for traditional GC and the proposed method is the same. TPVF, FPVF and accuracy (ACC) are used to show the segmentation performance differences. As shown in Table III, the proposed method shows significant improvements compared to the initialization results, traditional GC and GSGC ($p<0.05$). And it demonstrated that the proposed Bayesian based probability initialization can improve the GSGC segmentation performance. We also perform a correlation analysis between ground truth and the segmentation results (Fig. 12).The segmentation results have a strong a strong statistical correlation with ground truth ($r = 0.962$).

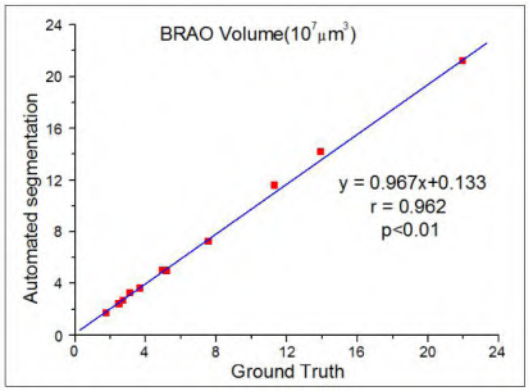

Fig. 12. Linear regression analysis comparing BRAO volumes of ground truth and segmentation results.

Because of there are misclassifications existing before the segmentation steps, to reduce miss detection, the GSGC base segmentation method and the model-based method are also performed on normal data. The experiment results show that there is no BRAO region detected on the true normal images. And BRAO regions can be detected on the false normal images (the image of BRAO acute phase misclassifed as normal in Table II, in this case, the image is re-classified as BRAO acute phase. Moreover, when normal images are mis-classified as BRAO, if there is no BRAO region detected, the image is re-classified as normal. Because there is no misclassification between BRAO acute and chronic phase (as shown in Table II), the re-classification step can correct all the misclassificaitons, achieving 100% accuracy.

V. CONCLUSION AND DISCUSSION

In this paper, we have proposed a framework to detect and segment BRAO region automatically based on 3D SD-OCT images. The proposed framework effectively differentiated BRAO into acute and chronic phase. The proposed method was tested on 35 SD-OCT images dataset consists of 12 patients of acute phase, 11 patients of chronic phase and 12 normal eyes. The classification accuracy of BRAO in acute phase and chronic phase were 100% and 90.9%, respectively. The overall TPVF and FPVF for acute phase were 91.1% and 5.5%; for chronic phase were 92.7% and 8.4%, respectively. The experiment results demonstrated the feasibility of the proposed method. Furthermore, this method generated the 2D projection of BRAO regions, which can provide shape, size and position information to aid the ophthalmologist's diagnosis.

The advantages of the proposed framework can be summarized as follows:

- This is the first paper that proposed to automatically segment BRAO in retinal 3D SD-OCT image. It is an important contribution in clinic.
- A novel BRAO classification method is proposed by combining local features (including structure, intensity and texture) with our new feature distribution analyzing

strategy, which can be applied in identifying of other local retinal diseases.
- The proposed method is validated on a clinical dataset showing high TPVF and low FPVF. The experimental results showed advantages to using GSGC method over the GC method for segmentation.
- Bayesian based probability initialization can improve the GSGC segmentation performance.

However, there are also some limitations for the proposed framework. The first limitation is that it largely relies on the layer segmentation results. If the layer segmentation is incorrect, it will affect the classification and segmentation of BRAO in chronic phase. Moreover, as can be seen from Fig. 9, the 2D projection of BRAO in chronic phase lacks a smooth boundary. Because of the thickness model (mean and standard deviation) varies in different position of retina, the BRAO segmentation results in 3D is not continuous between slices. The correlation analysis between the BRAO volume and the visual ability is also needed, which is very important to the clinical practice. The correlation issues will be investigated in a near future.

REFERENCES

[1] K. Hondeghem, M. Blanckaert, and J. Blanckaert, "Branch retinal artery occlusion in systemic diseases: A case report," *Bull. de la Societe belge d'ophtalmologie*, vol. 271, pp. 9–15, Dec. 1999.

[2] C. M. F. M. Parcero, B. D. P. Freitas, E. F. Marback, O. D. O. M. Júnior, and R. L. Marback, "Optical coherence tomography findings in acute phase of branch retinal artery occlusion: Case report," *Arquivos Brasileiros de Oftalmologia*, vol. 73, no. 2, pp. 189–192, 2010.

[3] S. S. Hayreh, "Acute retinal arterial occlusive disorders," *Prog. Retinal Eye Res.*, vol. 30, no. 5, pp. 359–394, 2011.

[4] J. O. Mason, III, A. A. Shah, R. S. Vail, P. A. Nixon, E. L. Ready, and J. A. Kimble, "Branch retinal artery occlusion: Visual prognosis," *Amer. J. Ophthalmol.*, vol. 146, no. 3, pp. 455–457, 2008.

[5] S. Rumelt and G. C. Brown, "Update on treatment of retinal arterial occlusions," *Current Opinion Ophthalmol.*, vol. 14, no. 3, pp. 139–141, 2003.

[6] R. K. Murthy, S. Grover, and K. V. Chalam, "Sequential spectral domain OCT documentation of retinal changes after branch retinal artery occlusion," *Clin. Ophthalmol.*, vol. 4, pp. 327–329, Apr. 2010.

[7] N. Yamaike *et al.*, "Three-dimensional imaging of cystoid macular edema in retinal vein occlusion," *Ophthalmology*, vol. 115, no. 2, pp. 355–362, Feb. 2008.

[8] S. Yun, G. Tearney, B. Bouma, B. Park, and J. de Boer, "High-speed spectral-domain optical coherence tomography at 1.3 μm wavelength," *Opt. Exp.*, vol. 11, no. 26, pp. 3598–3604, Dec. 2003.

[9] N. Goldenberg-Cohen *et al.*, "Molecular and histological changes following central retinal artery occlusion in a mouse model," *Experim. Eye Res.*, vol. 87, no. 4, pp. 327–333, Oct. 2008.

[10] H. Ozdemir, M. Karacorlu, S. A. Karacorlu, and F. Senturk, "Localized foveal detachment in a patient with central retinal artery occlusion with cilioretinal sparing," *Eur. J. Ophthalmol.*, vol. 22, no. 3, pp. 492–494, Jun. 2012.

[11] H. Chen *et al.*, "Quantitative analysis of retinal layers' optical intensities on 3D optical coherence tomography for central retinal artery occlusion," *Sci. Rep.*, vol. 5, p. 9269, Feb. 2015.

[12] C. K. S. Leung *et al.*, "*In vivo* measurements of macular and nerve fibre layer thickness in retinal arterial occlusion," *Eye*, vol. 21, no. 12, pp. 1464–1468, Jun. 2006.

[13] B. Asefzadeh and K. Ninyo, "Longitudinal analysis of retinal changes after branch retinal artery occlusion using optical coherence tomography," *Optometry*, vol. 79, no. 2, pp. 85–89, Feb. 2008.

[14] J. Xu, D. A. Tolliver, H. Ishikawa, G. Wollstein, and J. Schuman, "3D OCT retinal vessel segmentation based on boosting learning," in *World Congress on Medical Physics and Biomedical Engineering*, vol. 12, O. Dössel and W. Schlegel, Eds. Munich, Germany: Springer, 2009.

[15] H. Lu, N. Boonarpha, M. T. Kwong, and Y. Zheng, "Automated segmentation of the choroid in retinal optical coherence tomography images," in *Proc. Annu. Int. Conf. IEEE Eng. Med. Biol. Soc.*, Jul. 2013, pp. 5869–5872.

[16] M. M. Fraz, M. Y. Javed, and A. Basit, "Evaluation of retinal vessel segmentation methodologies based on combination of vessel centerlines and morphological processing," in *Proc. Int. Conf. Emerg. Technol.*, Oct. 2008, pp. 232–236.

[17] S. Fei *et al.*, "Automated 3-D retinal layer segmentation of macular optical coherence tomography images with serous pigment epithelial detachments," *IEEE Trans. Med. Imag.*, vol. 34, no. 2, pp. 441–452, Feb. 2015.

[18] W. Ding *et al.*, "Automatic detection of subretinal fluid and sub-retinal pigment epithelium fluid in optical coherence tomography images," in *Proc. Annu. Int. Conf. IEEE Eng. Med. Biol. Soc.*, Jul. 2013, pp. 7388–7391.

[19] D. Xu *et al.*, "A novel segmentation algorithm for volumetric analysis of macular hole boundaries identified with optical coherence tomography," *Investigative Ophthalmol. Vis. Sci.*, vol. 54, no. 1, pp. 163–169, 2013.

[20] Y. Y. Boykov and M.-P. Jolly, "Interactive graph cuts for optimal boundary and region segmentation of objects in ND images," in *Proc. Int. Conf. Comput. Vis.*, 2001, pp. 105–112.

[21] V. Kolmogorov and R. Zabih, "What energy functions can be minimized via graph cuts?" in *Proc. 7th Eur. Conf. Comput. Vis.*, 2002, pp. 65–81.

[22] V. Kolmogorov and R. Zabih, "Computing visual correspondence with occlusions using graph cuts," in *Proc. 8th IEEE Int. Conf. Comput. Vis.*, Jul. 2001, p. 508.

[23] X. Chen and U. Bagci, "3D automatic anatomy segmentation based on iterative graph-cut-ASM," *Med. Phys.*, vol. 38, no. 8, pp. 4610–4622, 2011.

[24] X. Chen, J. K. Udupa, A. Alavi, and D. A. Torigian, "GC-ASM: Synergistic integration of graph-cut and active shape model strategies for medical image segmentation," *Comput. Vis. Image Understand.*, vol. 117, no. 5, pp. 513–524, May 2013.

[25] Y. Boykov and V. Kolmogorov, "An experimental comparison of min-cut/max-flow algorithms for energy minimization in vision," *IEEE Trans. Pattern Anal. Mach. Intell.*, vol. 26, no. 9, pp. 1124–1137, Sep. 2004.

[26] S. Roy and I. J. Cox, "A maximum-flow formulation of the N-camera stereo correspondence problem," in *Proc. 6th Int. Conf. Comput. Vis.*, Jan. 1998, p. 492.

[27] X. Chen, J. K. Udupa, U. Bagci, Y. Zhuge, and J. Yao, "Medical image segmentation by combining graph cuts and oriented active appearance models," *IEEE Trans. Image Process.*, vol. 21, no. 4, pp. 2035–2046, Apr. 2012.

[28] Y. Boykov, O. Veksler, and R. Zabih, "Fast approximate energy minimization via graph cuts," *IEEE Trans. Pattern Anal. Mach. Intell.*, vol. 23, no. 11, pp. 1222–1239, Nov. 2001.

[29] K. Li, X. Wu, D. Z. Chen, and M. Sonka, "Optimal surface segmentation in volumetric images-a graph-theoretic approach," *IEEE Trans. Pattern Anal. Mach. Intell.*, vol. 28, no. 1, pp. 119–134, Jan. 2006.

[30] B. Appleton and H. Talbot, "Globally minimal surfaces by continuous maximal flows," *IEEE Trans. Pattern Anal. Mach. Intell.*, vol. 28, no. 1, pp. 18–106, Jan. 2006.

[31] L. Xiaomin, D. Z. Chen, M. H. Tawhai, W. Xiaodong, E. A. Hoffman, and M. Sonka, "Optimal graph search based segmentation of airway tree double surfaces across bifurcations," *IEEE Trans. Med. Imag.*, vol. 32, no. 3, pp. 493–510, Mar. 2013.

[32] M. K. Garvin, M. D. Abramoff, R. Kardon, S. R. Russell, W. Xiaodong, and M. Sonka, "Intraretinal layer segmentation of macular optical coherence tomography images using optimal 3-D graph search," *IEEE Trans. Med. Imag.*, vol. 27, no. 10, pp. 1495–1505, Oct. 2008.

[33] X. Chen *et al.*, "Quantitative analysis of retinal layer optical intensities on three-dimensional optical coherence tomography," *Investigative Ophthalmol. Vis. Sci.*, vol. 54, no. 10, pp. 6846–6851, 2013.

[34] X. Chen, M. Niemeijer, L. Zhang, K. Lee, M. D. Abràmoff, and M. Sonka, "Three-dimensional segmentation of fluid-associated abnormalities in retinal OCT: Probability constrained graph-search-graph-cut," *IEEE Trans. Med. Imag.*, vol. 31, no. 8, pp. 1521–1531, Aug. 2012.

[35] J. Guo *et al.*, "A framework for classification and segmentation of branch retinal artery occlusion in SD-OCT," *Proc. SPIE*, vol. 9784, p. 978425, Mar. 2016.

[36] E. Gao *et al.*, "Comparison of retinal thickness measurements between the topcon algorithm and a graph-based algorithm in normal and glaucoma eyes," *PLoS ONE*, vol. 10, no. 6, p. e0128925, May 2015.

[37] Q. Sun, J. A. Hossack, J. Tang, and S. T. Acton, "Speckle reducing anisotropic diffusion for 3D ultrasound images," *Comput. Med. Imag. Graph.*, vol. 28, no. 8, pp. 461–470, 2004.
[38] P. Perona and J. Malik, "Scale-space and edge detection using anisotropic diffusion," *IEEE Trans. Pattern Anal. Mach. Intell.*, vol. 12, no. 7, pp. 629–639, Jul. 1990.
[39] S. Aja-Fernandez and C. Alberola-Lopez, "On the estimation of the coefficient of variation for anisotropic diffusion speckle filtering," *IEEE Trans. Image Process.*, vol. 15, no. 9, pp. 2694–2701, Sep. 2006.
[40] X. Zhang, L. Li, F. Zhu, W. Hou, and X. Chen, "Spiking cortical model-based nonlocal means method for speckle reduction in optical coherence tomography images," *J. Biomed. Opt.*, vol. 19, no. 6, p. 066005, 2014.
[41] S. T. Acton, "Speckle reducing diffusion for ultrasound image enhancement using the structural similarity image measure," in *Proc. IEEE 5th Int. Workshop Comput. Adv. Multi-Sensor Adaptive Process. (CAMSAP)*, Dec. 2013, pp. 153–156.
[42] J. Weickart, "Anisotropic diffusion in image processing," *Teubner Stuttgart*, vol. 16, no. 1, p. 272, 1996.
[43] G. Quellec, K. Lee, M. Dolejsi, M. K. Garvin, M. D. Abràmoff, and M. Sonka, "three-dimensional analysis of retinal layer texture: Identification of fluid-filled regions in SD-OCT of the macula," *IEEE Trans. Med. Imag.*, vol. 29, no. 6, pp. 1321–1330, Jun. 2010.
[44] Y. Freund and R. E. Schapire, "Experiments with a new boosting algorithm," in *Proc. 13th Int. Conf. Mach. Learn.*, 1996, pp. 148–156.
[45] J. K. Udupa *et al.*, "A framework for evaluating image segmentation algorithms," *Comput. Med. Imag. Graph.*, vol. 30, no. 2, pp. 75–87, Mar. 2006.
[46] Y. Boykov and G. Funka-Lea, "Graph cuts and efficient N-D image segmentation," *Int. J. Comput. Vis.*, vol. 70, no. 2, pp. 109–131, Nov. 2006. [Online]. Available: http://dx.doi.org/10.1007/s11263-006-7934-5

Jingyun Guo, photograph and biography not available at the time of publication.

Weifang Zhu, photograph and biography not available at the time of publication.

Fei Shi, photograph and biography not available at the time of publication.

Dehui Xiang, photograph and biography not available at the time of publication.

Haoyu Chen, photograph and biography not available at the time of publication.

Xinjian Chen, photograph and biography not available at the time of publication.